

See discussions, stats, and author profiles for this publication at: <https://www.researchgate.net/publication/272328891>

CHP-Integrated Fischer-Tropsch Biocrude Production under Norwegian Conditions: Techno-Economic Analysis

ARTICLE in ENERGY & FUELS · JANUARY 2015

Impact Factor: 2.79 · DOI: 10.1021/ef502326g

READS

15

6 AUTHORS, INCLUDING:



Rajesh S Kempegowda

SINTEF

12 PUBLICATIONS 145 CITATIONS

[SEE PROFILE](#)



Gonzalo Del Alamo

SINTEF

9 PUBLICATIONS 77 CITATIONS

[SEE PROFILE](#)



Mette Bugge

SINTEF

6 PUBLICATIONS 11 CITATIONS

[SEE PROFILE](#)



Khanh-Quang Tran

Norwegian University of Science and Technol...

41 PUBLICATIONS 613 CITATIONS

[SEE PROFILE](#)

CHP-Integrated Fischer-Tropsch Biocrude Production under Norwegian Conditions: Techno-Economic Analysis

Rajesh S Kempegowda,^{*,†} Gonzalo del Alamo,[‡] David Berstad,[‡] Mette Bugge,[‡] Berta Matas Güell,[‡] and Khanh-Quang Tran[†]

[†]Department of Energy & Process Engineering, NTNU, Trondheim, Norway

[‡]SINTEF Energy Research, Trondheim, Norway

Supporting Information

ABSTRACT: This article presents a detailed techno-economic analysis, under Norwegian conditions, for the production of biocrude from woody biomass via high temperature entrained flow gasification and Fischer–Tropsch (FT) synthesis with integrated coproduction of heat and electricity. Biomass pretreatment based on both conventional drying and torrefaction processes are considered as options. Maximum calculated efficiency of biocrude at lower and upper bound CO conversions of 40% and 80% at the gasifier operating conditions of lambda value 0.2 and temperature 1300 °C are 27% and 44%, respectively. Under these conditions, maximum thermal and net electrical efficiency are 55% and 15.5%, respectively. The economic viability of the biocrude production for plant capacities in the range of 150–600 MW thermal input has been evaluated as a function of the type of biomass pretreatment, gasification operating conditions, and the heat to electricity production ratios. Results from the economic analysis show that coproduction of biocrude combined with 100% heat production for district heating gives the lowest biocrude cost under Norwegian conditions, with large variations as the electricity to heat production ratio increases.

1. INTRODUCTION

The worldwide consumption of liquid fuels for transportation is continuously increasing and is likely to double between 2000 and 2050.¹ At the same time, there is a gradual decrease in the known reserves of fossil-fuel feedstock. This decrease is coupled with an increase in the emissions of greenhouse gases, mainly CO₂, these being responsible for global warming. Hence, there is a need to develop methods to decrease total global greenhouse gas emissions. It is widely accepted that an important aspect in the mitigation efforts of climate change is the use of renewable fuel sources. This has led to an increasing interest in the use of biofuels. The *EU Renewables Directive*² has put forward the 20/20/20 targets to combat greenhouse gas emissions. This Directive also includes targets for the transport sector: to reach a 10% share of renewable energy by 2020, whereof a substantial part should be biofuels. Estimates carried out by Eurostat³ states that around 25% of Europe's transport energy demand will be supplied by advanced sustainable biofuels in 2030, saving over 90 million tonnes of mineral oil per year, while the IEA⁴ roadmap envisions that by 2050, 32 EJ of biofuels will be used globally, providing 27% of the world transport fuel need. A recent Norwegian study⁵ shows that biofuels may be expected to be the second most important contributor to lower greenhouse gas emissions from the Norwegian transport sector in the future. This message is coherent with recently established policies, both Norwegian^{6,7} and international (e.g., the *EU Renewables Directive*).² Presently, the requirement is that 3.5% of the total fuels used for road transport in Norway shall be biomass-derived.

Currently, biofuels are produced at commercial scale mainly from biomass resources which are also competing with food supply, using the so-called “First Generation Biofuel” technologies.⁸ In achieving commercialization on a large scale,

first generation biofuels appear to have many shortcomings, which include land-use conflict, increasing food prices, and limited CO₂ reduction.^{9,10} In order to overcome these issues, the so-called “Second Generation Biofuel” technologies¹¹ for the production of transport fuels from a wide range of lignocellulosic biomass feedstock, noncompeting with food supply, have been proposed. Among second generation biofuels, biodiesel produced via biomass gasification and Fischer–Tropsch (FT) synthesis has gained particular interest since it has a similar fuel quality to fossil-derived diesel. However, despite the numerous resources and extensive research work worldwide on developing FT biodiesel production technologies during the past few decades, the progress in industrialization and commercialization of second generation biofuels has been very limited. This is mainly due to the low biomass-to-biodiesel conversion efficiency and the large scale of the plant required in order to make it cost-effective. This requirement may be even more critical for countries like Norway, where lignocellulosic biomass is dispersed and, therefore, the costs and environmental impact of biomass transport is significant. In this context, pretreatment of lignocellulosic biomass via torrefaction for production of FT biodiesels can improve the overall conversion economics since it increases the energy density of the feedstock and, therefore reduces transportation costs and increases conversion efficiencies.

Extensive research work is available in the literature addressing the improvement of biomass feedstock quality via torrefaction pretreatment processes. The following main improvements in the biomass properties after torrefaction

Received: October 15, 2014

Revised: January 29, 2015

Published: January 29, 2015



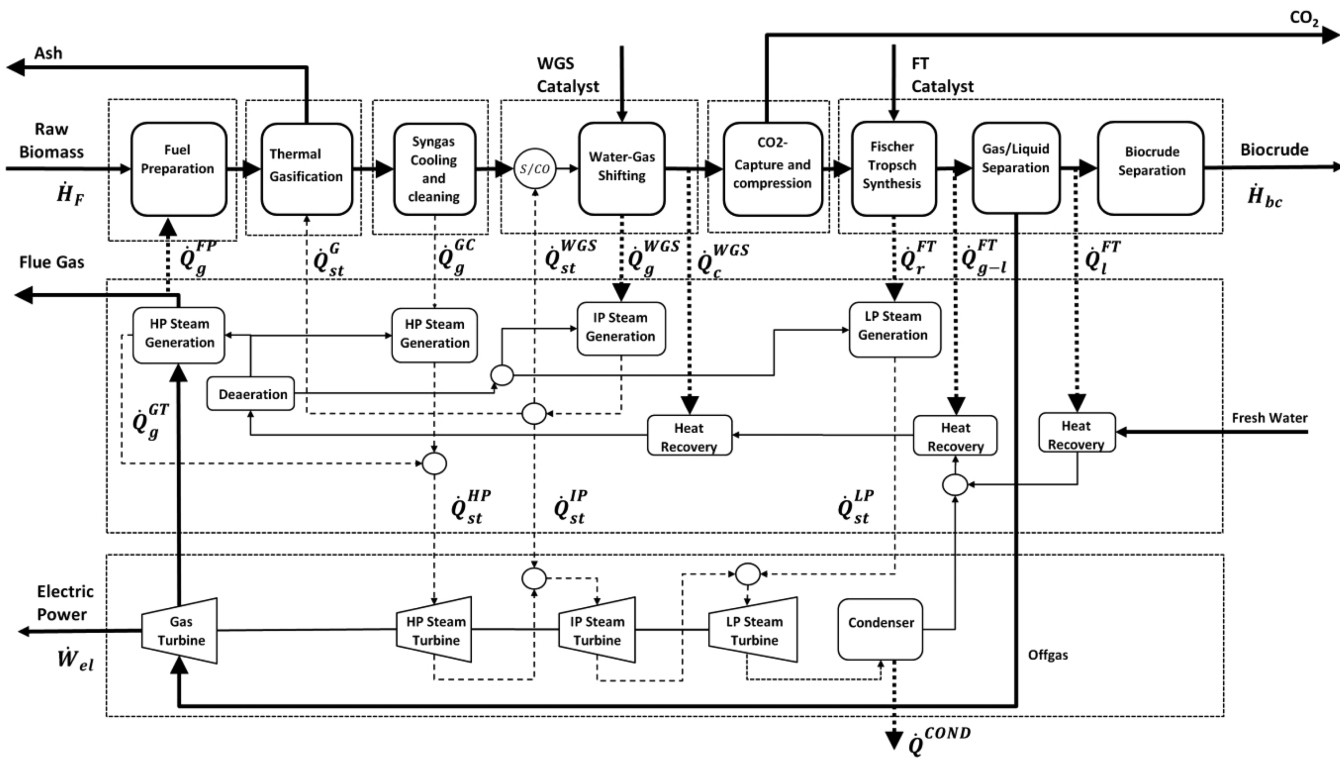


Figure 1. BTL plant process diagram.

have been reported: (i) considerable reduction in the moisture content,^{12,13} (ii) increased energy density and heating value due to reduction in the O/C ratio,^{14–16} (iii) intrinsic conversion of the hygroscopic behavior of raw biomass into the hydrophobic behavior of torrefied biomass,¹⁷ and (iv) enhanced grindability, which results in less energy consumption during milling.^{18,19}

In addition, the integration of CHP production in FT synthetic fuels production plants based on recovery of residual energy from the syngas cooling after gasification, the exothermic WGS and FT processes, and from the off-gas produced from biocrude separation has also been included to improve the energy efficiency and the economic viability of FT biofuels production (Swanson et al.,²⁰ Värmeforsk,²¹ and Tijmensen et al.²²).

The present work investigates the influence of biomass thermal pretreatment, under Norwegian conditions, and the main operational parameters of gasification on the overall energy efficiencies in a CHP-integrated FT biocrude production plant. The main biocrude production process involves feed preparation, including drying or torrefaction and particle size reduction, high temperature entrained flow gasification, syngas cooling and conditioning, CO₂ capture and compression, FT synthesis, and separation of biocrude. The plant process design also involves optimized heat recovery and steam generation from the main process and electric power production in order to improve the overall efficiency and economics of the plant. Further refining of the biocrude is excluded from the analysis. The process analysis of the plant is performed by using Aspen Plus for plant capacity in the range of 150 to 600 MW input biomass energy rate. This range is considered to be relevant under Norwegian conditions based on the typical capacities of thermal networks for exporting the waste heat from the plant, the biomass availability, and the capacity of commercially available EF gasification systems. The

focus is to produce FT crude with CHP as a coproduct using commercially available FT technology. Parametric expressions are also derived for the main energy flows and efficiencies based on fuel properties, composition of the syngas produced from gasification, and the main process design parameters. Results of capital costs, cost of biocrude, and return on equity or financial internal rate of return (FIRR) for investors are evaluated to study the plant viability under Norwegian conditions.

2. PROCESS ANALYSIS

2.1. Plant Process Design. Figure 1 shows the process flow diagram for the CHP-integrated biocrude production plant studied in this work. The main process steps for the biomass to biocrude conversion are (i) fuel preparation, (ii) high-temperature and oxygen-enriched EF gasification, (iii) syngas cooling, (iv) water–gas shifting (WGS), (v) CO₂ separation and compression, and (vi) Fischer–Tropsch (FT) synthesis including gas and biocrude separation. In addition, available heat from the syngas cooling, off-gas combustion, water–gas shifting, and Fischer–Tropsch synthesis is recovered for combined heat and power (CHP) production. A more detailed description of each system, including main process design and operational parameters, is presented below.

Feedstock Preparation. Norwegian raw birch chips are used as input fuel to the plant. A representative characterization of Norwegian raw birch,²³ including proximate and ultimate analysis and heating values, is shown in Table 1. The input birch chips have typically a maximum moisture content of 50% (wt) and typical average particle size of 40 mm. Therefore, fuel preparation is needed in order to reduce the moisture content and the particle size to the requirements of the entrained flow gasification, denoted respectively by $\delta_{H_2O,F}^{FP}$ and $\delta_{p,F}^{FP}$. Two different steps for moisture reduction are included in the analysis, one based on dry torrefaction and the other on

Table 1. Biomass Characteristics (Proximate and Ultimate Analysis, Heating Values and Yields) for Raw and Pretreated Norwegian Woodchips

input fuel	birch, raw	birch, torrefied (at 275 °C during 30 min)
volatiles (% wt dry)	89.43	77.14
fix carbon (% wt dry)	10.35	22.64
ash (% wt dry)	0.22	0.22
LHV (MJ/kg dry)	18.42	19.29
C (% w/w)	48.62	55.55
H (% wt dry)	6.34	5.77
O (% wt dry)	44.9	38.5
N (% wt dry)	0.09	0.13
S (% wt dry)	0.05	0.05

conventional thermal drying. Particle size reduction after moisture reduction is performed for both cases in a grinder. A schematic representation of the two fuel preparation processes is shown in Figure 2.

The overall biomass torrefaction system is designed to be thermally self-sustained based on combustion of volatiles released during the torrefaction process itself. For the biomass drying process, the flue gas coming from the FT combined cycle, at temperature $T_{g,0}^{\text{FD}}$, is utilized as the heating medium. This temperature is specified to be 130 °C in order to avoid biomass autoignition in the drier. The particle size for EF gasification is specified to be 1 mm, which has been reported to be an optimum trade-off value between the energy consumed for grinding and the performance of the gasification process.²⁴

Gasification System. Oxygen-enriched EF gasification at high temperatures is the technology chosen for the biomass thermal conversion. This technology exhibits a number of advantages for integration into biofuels production via FT synthesis relative to fixed-bed or fluidized-bed gasification: the high gas temperature in the reactor causes melting of the ash and, in the presence of steam, enhances thermal reforming of hydrocarbons, water–gas shifting of carbon monoxide increasing the hydrogen content, and thermal cracking of tars.²⁵ The overall EF gasification process can then be described in terms of the gasification reactor pressure and temperature, the λ value or air-fuel equivalence ratio, and the steam to carbon ratio, denoted respectively by P_g^G , T_g^G , λ_g and $(S/C)_g$. Here, the λ value is defined as the ratio between the actual molar flow rate of oxygen used for gasification to the total stoichiometric flow rate needed for complete biomass combustion. Lower and upper operational limits for the gas temperature in the entrained flow gasification are specified with constant values equal to 1300 and 1600 °C, respectively. The lower

temperature limit is specified in order to ensure complete ash melting.²⁶ The upper temperature limit corresponds to technical constraints in refractory materials which are commercially available at reasonable prices. The range of variation for λ_g is assumed to be between 0.2 and 0.4. This is has been established as an optimal range for oxygen-enriched gasification²⁷ to achieve complete char gasification as well as partial oxidation of the high-chain hydrocarbons and polycyclic aromatic hydrocarbons produced during decomposition of the volatile fraction of the biomass. The oxygen-enriched air flow rate required for the EF gasification, with O₂ concentration denoted by $X_{\text{O}_2}^{\text{ASU}}$, is produced in an air separation unit (ASU) and then compressed to gasification pressure.

Syngas Cooling. A direct syngas cooling system is chosen in this work, where the thermal enthalpy of the syngas leaving the gasification process is utilized for production of superheated steam at high pressure and temperature conditions, denoted by $P_{\text{stm}}^{\text{HP}}$ and $T_{\text{stm}}^{\text{HP}}$. The process design for the syngas cooling system is shown in Figure 3. Initially, the syngas is cooled in a radiation wall followed by a water-tube evaporator, where the saturated water from a flash tank is partially evaporated to saturation conditions. The radiation wall has been chosen due to the high temperature of the gas produced from the EF gasification, so that the design temperature of the tube bundles in the evaporator is reduced. The syngas is then further cooled in a superheater, where the temperature of saturated steam coming from the flash tank is increased, followed by cooling in a smoke-tube boiler, where complete vaporization of steam is achieved. The final step in cooling the syngas is performed in an economizer to increase the temperature of the feedwater. The temperature of the syngas after the economizer is specified as the minimum inlet temperature to the water–gas shifting required for activation of the catalysts, represented by $T_{g,0}^{\text{WGS}}$.

Water–Gas Shifting. The H₂ to CO molar ratio of the syngas leaving the gasification reactor is typically below the H₂ to CO molar ratio required for optimum FT synthesis. In order to increase the H₂/CO ratio, a catalytic WGS stage is included. Figure 4 shows the process diagram for the water–gas shifting with integration of heat recovery and steam generation. In order to minimize the reactor and catalyst volume, and thus reduce costs, only a fraction λ_{wgs} of the total molar flow rate of the syngas leaving the gasification unit undertakes complete WGS. Prior to the WGS reactor, mixing of the syngas stream with additional steam at intermediate pressure increases the steam to CO molar ratio to the value required by the WGS, here defined by $(S/\text{CO})_{\text{WGS}}$. According to available data in the literature on the performance of commercial WGS catalysts,²⁰ optimum values of the steam to CO molar ratio are between 1

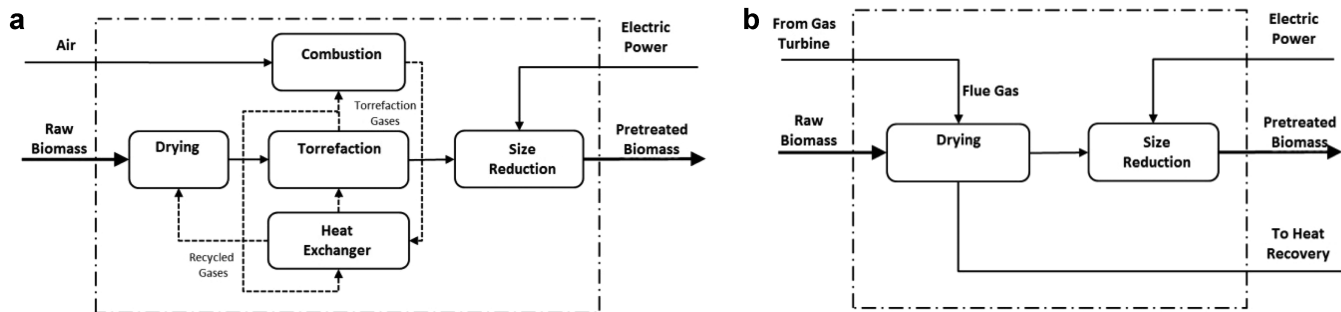


Figure 2. Schematic process diagram for the biomass pretreatment based on (a) dry torrefaction and (b) conventional drying.

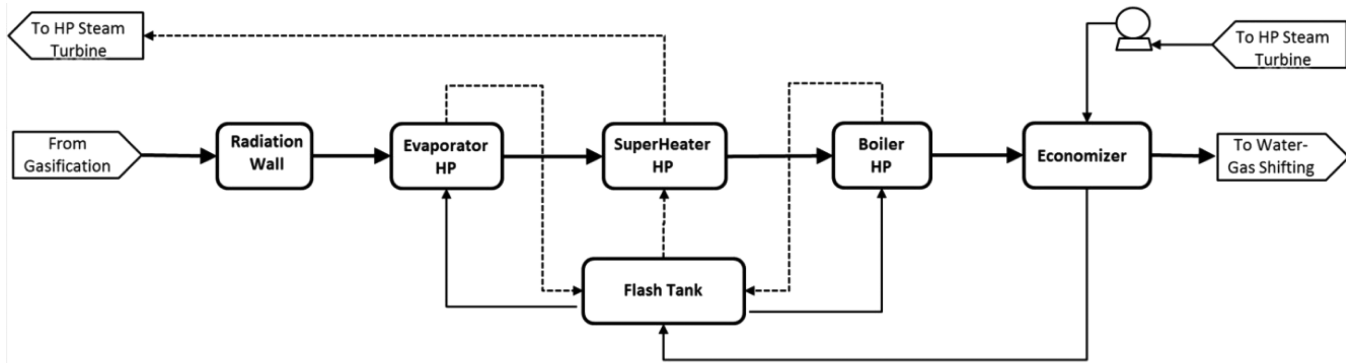


Figure 3. Schematic representation of the syngas cooling with integration of heat recovery steam generation.

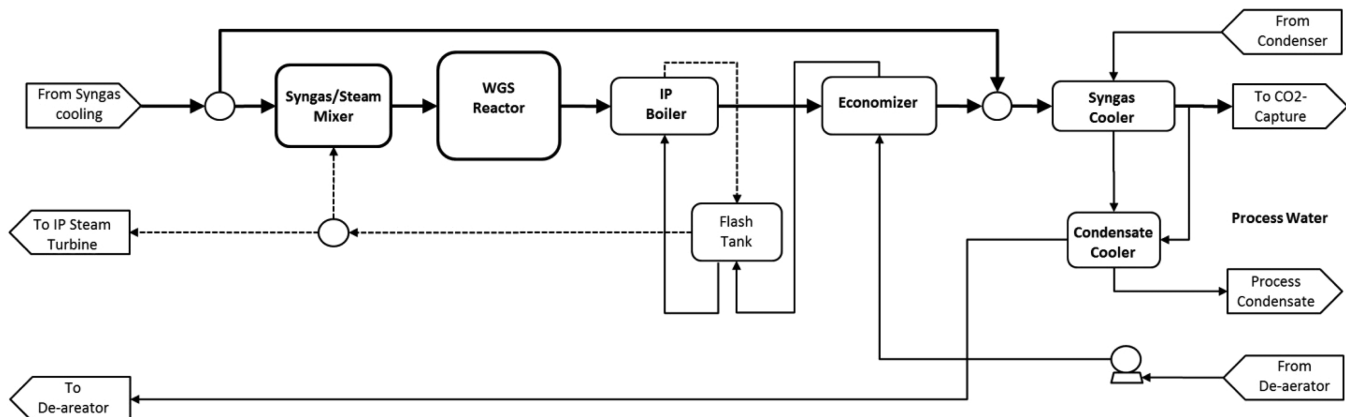


Figure 4. Process flow diagram for water-gas shifting and integrated heat recovery and steam generation.

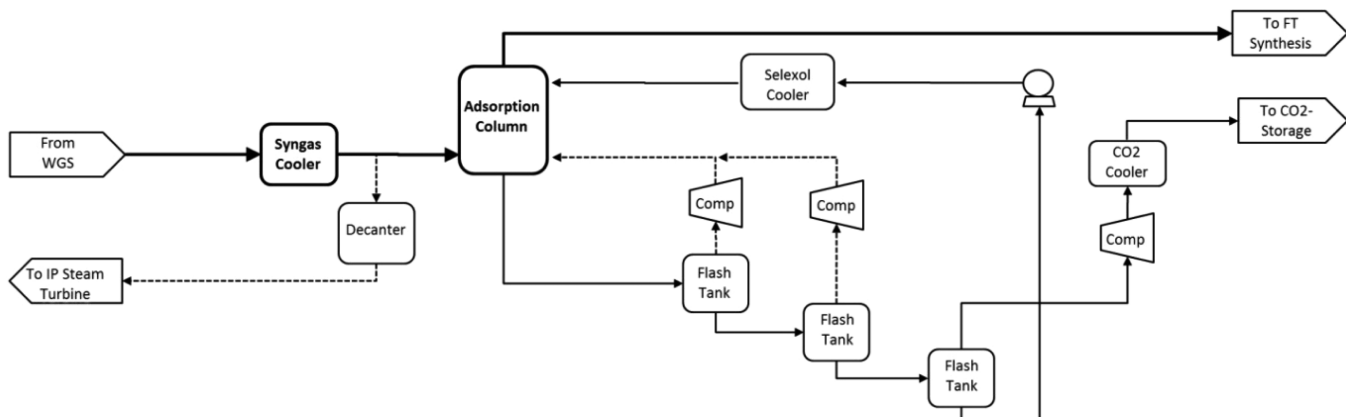


Figure 5. Selexol CO₂ separation unit.

and 1.2 for optimum CO to H₂ conversion and catalyst utilization. Adiabatic reactors for WGS are chosen in the present analysis, followed by syngas cooling with heat recovery through a boiler, for generation of saturated steam at intermediate pressure, and an economizer for preheating of the feedwater. Adiabatic reactors have been chosen for WGS under the assumption of having simpler designs with lower fabrication and maintenance costs. Also, adiabatic WGS leads to higher gas temperatures which allow more efficient heat recovery with lower heat transfer area. When considering adiabatic reactors, the gas temperature from the WGS, denoted by T_r^{WGS} , must be limited so that the WGS reaction rate is sufficiently high to achieve complete CO conversion with short residence times. According to existing investigations²⁸ on

commercial catalysts, complete CO conversion can be achieved for temperatures below 600 °C. Above this temperature, an additional reactor is required to achieve complete WGS shifting. This has implications only on the techno-economic analysis of the plant but not for the overall energy efficiency of the plant. Heat recovery from the WGS reactor is performed using a boiler for steam generation and an economizer for increasing the temperature of the feeding water. The temperature of the syngas after the economizer is kept above the saturation temperature to avoid water condensation. The total syngas flow after mixing the bypassed and shifted syngas streams then passes through a cooler so that the syngas temperature decreases as much as possible prior to the CO₂ capture. The heat recovered from this cooler is utilized to heat

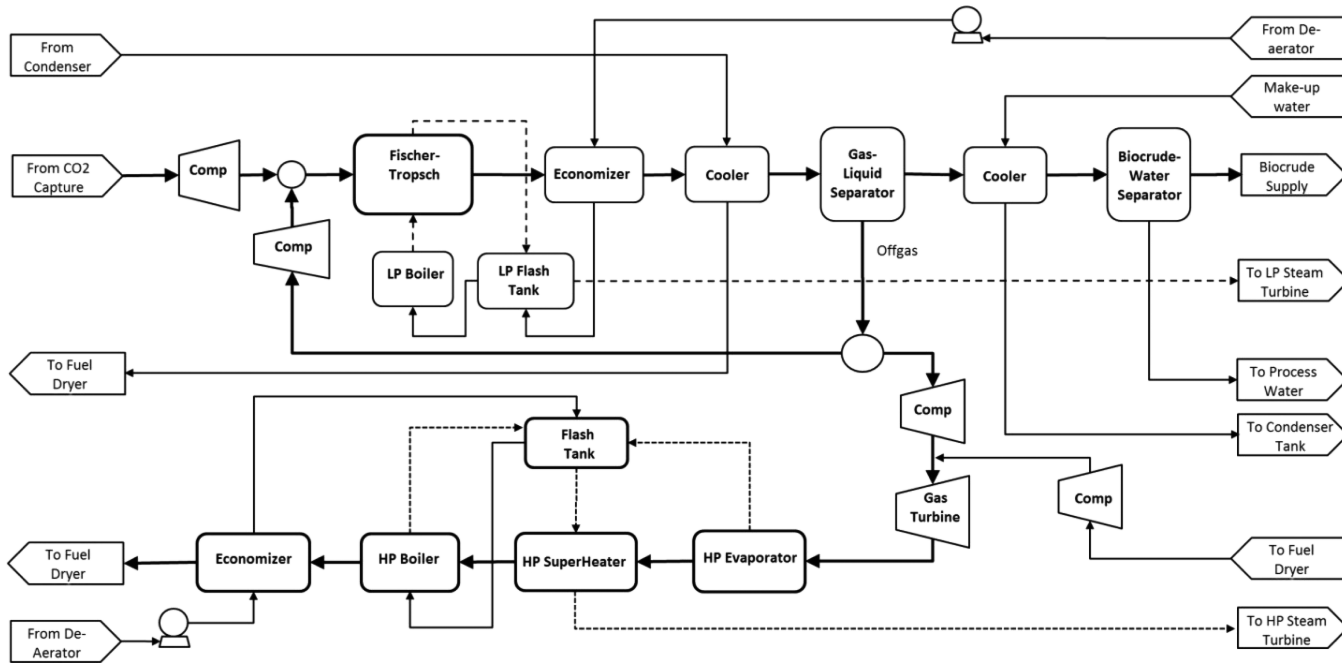


Figure 6. Heat recovery in Fischer–Tropsch reactor.

up the return condensate coming from the steam condenser before deaeration. An additional cooler has been included to recover heat from the water condensed during the syngas cooling, also utilized for heating up the return condensate.

CO₂ Capture and Compression. After WGS, the CO₂ concentration of the syngas is typically 21–35%. Therefore, CO₂ capture is required in order to reduce the CO₂ concentration of the syngas to the level needed for FT synthesis, denoted by $x_{\text{CO}_2}^{\text{CCS}}$, which is here specified to be 5%. The required CO₂ removal efficiency then varies from 82 to 90%, depending on the initial syngas composition, while the pressure of the outlet CO₂ stream is specified to be close to atmospheric. Furthermore, H₂ and CO losses during the CO₂ removal should be minimized in order to retain the desired H₂/CO ratio for FT synthesis. Considering these requirements, CO₂ capture based on physical solvents²⁹ has been selected as the optimal technology. The reason for this is mainly the relatively high CO₂ partial pressure, which is well within the application range for physical solvents, but also the relatively moderate CO₂ removal efficiencies. Among the physical solvents available commercially, Selexol has been chosen as it allows pure pressure-swing process configurations without the need for solvent refrigeration or thermal regeneration in the range of CO₂ removal efficiencies considered. This enables substantial savings in energy consumption.

The process flow diagram of the CO₂ removal process is shown in Figure 5. The syngas after WGS is initially water-cooled to 25 °C, and free water is removed in a water knockout drum. The syngas then enters the absorber where it is in contact with the Selexol solvent, also precooled to 25 °C by cooling water. The rich solvent is then regenerated in three flash drums, operating at 10, 6.5, and 1.1 bar. The flash gas from the first two flash drums contains considerable amounts of hydrogen and CO and is therefore recycled to the absorber to minimize the losses of these components. The flashed gas from the near-atmospheric regeneration stage is a high-purity CO₂

stream which is further compressed and cooled to $P_{\text{CO}_2}^{\text{CCS}}$ and $T_{\text{CO}_2}^{\text{CCS}}$ for storage.

Fischer–Tropsch Synthesis. Figure 6 shows the process design for FT synthesis integrated with a CHP system. The syngas stream after CO₂ capture is compressed by a booster compressor and fed into the FT reactor. The FT synthesis process is here specified based on the pressure and temperature along the catalyst bed, denoted by P_r^{FT} and T_r^{FT} , the CO conversion factor γ_r^{FT} and products selectivity. In terms of technology, a low-temperature FT synthesis (LTFT) in a slurry phase reactor with conventional cobalt catalyst has been chosen in this work. State-of-the-art LTFT synthesis using CO-based catalysts has been proven on a commercial scale³⁰ to achieve up to 80% CO conversion^{30,31} and to maximize the production of waxes,³² which is desirable for the production of high-quality diesel fuels.³³ CO-based catalysts have also been shown to exhibit high resistance to deactivation. For these types of catalysts, the optimal syngas H₂/CO ratio is typically in the range of 1.1–1.2.

The FT synthesis is highly exothermic, with the total heat of reaction representing approximately 25% of the total calorific value of the syngas. Therefore, it is very important to efficiently remove the heat released from the FT synthesis³⁴ in order to achieve uniformity of the temperature inside the reactor. This avoids problems with catalyst deactivation due to sintering and coking³⁵ as well as formation of significant amounts of undesirable methane in the product through methanation.³³ As shown in Figure 6, this work considers an integrated water-tube boiler in the FT reactor with steam generation at low pressure (LP). Since the heat transfer coefficient in the boiling regime is high, this design allows effective cooling of the catalyst bed.

The product stream from the FT reactor is cooled to temperature T^{GS} prior to gas separation. Cooling occurs in two stages: an economizer, which preheats the feedwater to the LP boiler, followed by a cooler for heating up the return condensate from the turbine condenser. After the gas/liquid

separation, the water and biocrude mixture is further cooled for separation of the biocrude, which occurs at temperature T^{BS} . In order to improve the overall efficiency of biocrude production, a fraction α_g^{FT} of the off-gas released from the gas/liquid separation is compressed and recirculated back to the FT reactor. The remaining off-gas stream, not recirculated to FT synthesis, is compressed and combusted in a gas turbine for electric power production. The flue gas from the gas turbine is used for generation of superheated steam at high pressure (HP). This steam generation scheme is similar to the one used for the syngas cooling, including an evaporator, superheater, high-pressure boiler, and economizer. The remaining thermal enthalpy of the flue gas leaving the economizer is then utilized for drying of the raw biomass in the fuel preparation system. The gas temperature at the outlet of the economizer is specified to be 130 °C, to avoid reaching flammability during fuel drying. The combustion and expansion processes in the gas turbine are characterized by the moles of combustion air per mole of off-gas, denoted by ϕ , the pressure ratio between the inlet flue gas after combustion of the off-gas stream and the outlet, denoted by r_{GT} , and the compression ratio for the combustion air $r_{air,c}$.

Steam Cycle. The HP, IP, and LP steam produced from the main conversion process is then utilized for electricity production in a three-stage steam turbine. The performance of each stage of the steam turbine are defined by the isentropic efficiencies, denoted by η_S^{HP} , η_S^{IP} , and η_S^{LP} . The saturated steam is leaving the LP stage of the steam turbine at back pressure P_0^{LP} and then cooled in a condenser. The return condensate from the LP steam turbine and fresh makeup water are mixed, heated up using residual process water, deaerated at pressure P_{fw} and temperature T_{fw} , and then fed pumped at high, intermediate, and low pressure for steam production.

2.2. Process Simulation and Results. Modeling and simulation of the CHP-integrated biocrude production plant have been performed using Aspen Plus. In general, built-in process models and physical/chemical property databases are used, complemented by user-defined functions in FORTRAN for modeling specific subprocesses and streams. Table 2 lists the design process parameters used for the simulations. The input biomass feedstock is defined by the proximate and ultimate analysis. The net calorific value of the biomass is estimated from the composition using a correlation recently published by Vhatthavarothai et al.³⁶ For modeling the biomass gasification process, the moisture and volatiles fractions of the biomass are first decomposed into elementary atomic components (C, H, O, N, and S) in the gas phase. Then, thermochemical equilibrium based on Gibbs free energy minimization is calculated for the elementary gas system and the solid carbon (char) subject to the following reaction mechanism:³⁷



The product selectivity for the Fischer–Tropsch synthesis is described using the ASF (Anderson–Schulz–Flory) model for the *n*-paraffins,³⁸ where α , the chain growth probability factor, is assumed to be a constant dependent only on the type of

Table 2. Specification of Process Design Parameters Used in the Analysis

process parameter	value
raw biomass moisture (max), $y_{H_2O,F}$	50%
biomass moisture after pretreatment, $y_{H_2O,F}^{FP}$	5%
biomass particle size after pretreatment, $\delta_{p,F}^{FP}$	3 mm
EF gasification pressure, P_g^G	25 bar-g
EF gasification temperature, T_g^G	1300–1600 °C
gasification λ value, λ_g	0.2–0.4
ASU outlet O ₂ concentration, $x_{O_2}^{ASU}$	95%
inlet syngas temperature to WGS, $T_{g,0}^{WGS}$	160 °C
maximum temperature WGS, T_r^{WGS}	600 °C
max. temperature difference gas/liquid coolers	10 °C
syngas CO ₂ concentration after CO ₂ capture, $x_{CO_2}^{CCS}$	5% vol.
CO ₂ supply pressure, $P_{CO_2}^{CCS}$	100 bar-g
CO ₂ supply temperature, $T_{CO_2}^{CCS}$	30 °C
FT reactor temperature, T_r^{FT}	250 °C
FT reactor pressure, P_r^{FT}	25–40 bar-g
FT synthesis progress (CO conversion factor) γ_r^{FT}	40–80%
FT off-gas recirculation, α_g^{FT}	40%
FT gas separation temperature, T^{GS}	95 °C
FT biocrude separation temperature, T^{BS}	45 °C
feed water temperature after deaeration, T_{fw}	105 °C
steam high pressure (HP), P_{stn}^{HP}	80 bar-g
steam superheated temperature (HP), T_{stn}^{HP}	580 °C
steam intermediate pressure (IP), P_{stn}^{IP}	25 bar-g
steam low pressure (LP), P_{stn}^{LP}	10 bar-g
gas turbine pressure, P_g^{GT}	25 bar-g
flue gas temperature to fuel drier, $T_{g,i}^{FD}$	130 °C

catalysts and independent of the chain length and gas conditions. The Peng–Robinson equation of state with Boston–Mathias alpha function (PR–BM) is used to estimate all physical properties (Aspen Technology, 2008) for the gasification and downstream unit operations.

Operational Limits in EF Gasification. Figure 7 shows the operational limits of the EF gasification for both dried and torrefied biomass, represented as the variation of the S/C ratio with the lambda value for the lower and upper temperature limits. The steam to carbon ratio increases linearly with increasing λ value (Figure 7a), with higher values for torrefied biomass relative to dried biomass due to the higher calorific value. Figure 7b shows the variation of the H₂ to CO molar ratio of the syngas leaving the EF gasification for the operational limits. These results show that lower gasification temperatures lead to higher H₂/CO molar ratio. Figure 7b also shows that gasification of dried biomass produced syngas with higher H₂/CO ratios than torrefied biomass, particularly at lower air–fuel equivalence ratios (λ_g). This can be explained due to the higher H content of the dried biomass.

Biocrude Production Efficiency. Figure 8 shows the efficiency of biocrude production relative to the total biomass input, based on the higher heating value, for the operational limits of the EF gasification and for both dried and torrefied biomass. Biocrude efficiency was estimated at two levels of CO conversion, 40% and 80% as shown in Figure 8a and b. In general, the biocrude production decreases with increasing values of λ_g due to increased oxidation of the syngas. However, the influence of the biomass pretreatment and the gasification temperature on the biocrude production exhibit different trends. For equivalence ratios (λ_g) lower than approximately

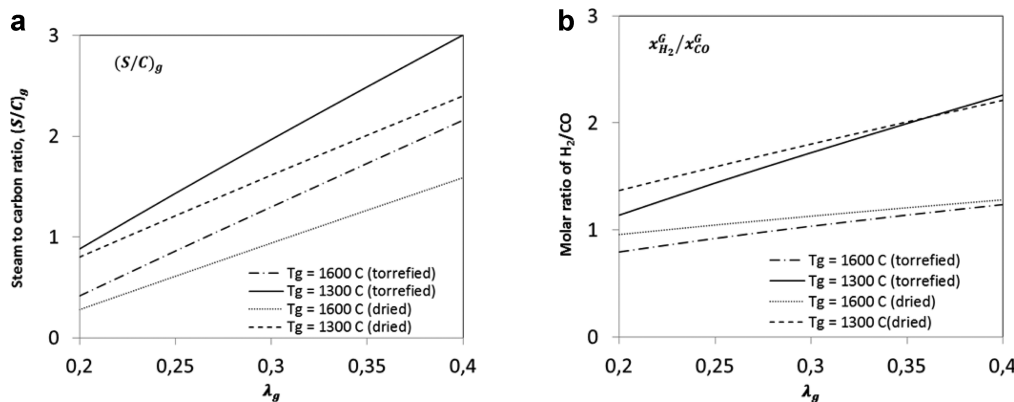


Figure 7. Variation of the steam to carbon ratio (a) and the outlet syngas H_2/CO molar ratio (b) with the air–fuel equivalence ratio (λ_g) for gasification of dried and torrefied biomass in the entrained-flow reactor for the lower and upper temperature limits.

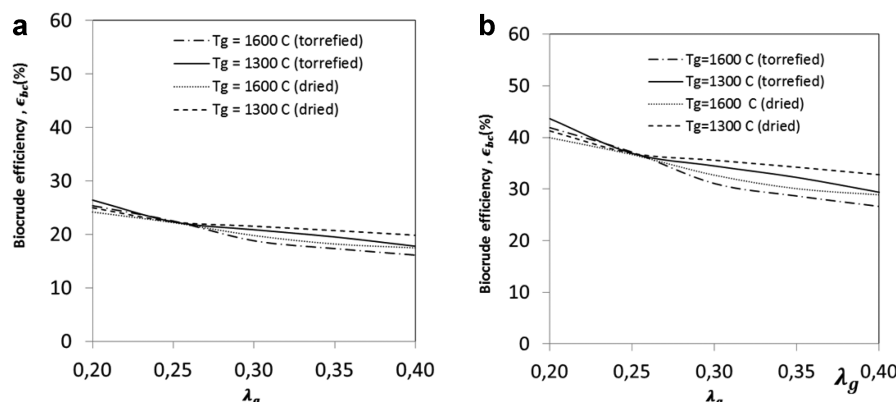


Figure 8. Variation of the biocrude efficiency with the gasification operating λ_g and temperature (1300–1600 C) for dried and torrefied biomass.

0.25, the biocrude production is higher for the torrefied biomass than for dried biomass for the range of gasification temperatures considered. As the equivalence ratio (λ_g) increases, the effect of biomass feedstock and gasification temperature becomes more relevant, with a higher rate of biocrude production for dried biomass and at lower temperatures.

Thermal Efficiency. Figure 9a shows the variation of the net thermal efficiency, denoted by ϵ_{th} , within the operational range of the EF gasification and for both dried and torrefied biomass. The net thermal efficiency is here calculated from $\epsilon_{th} = (\dot{Q}_{stn}^{HP} + \dot{Q}_{stn}^{IP} + \dot{Q}_{stn}^{LP})/\dot{H}_F$, where \dot{Q}_{stn}^{HP} , \dot{Q}_{stn}^{IP} , and \dot{Q}_{stn}^{LP} are the net steam production at high, intermediate, and low pressure, respectively, and $\dot{H}_F = \dot{M}_F NCV_F$ is the rate of input biomass energy to the plant. Figure 9c,d shows the contribution from \dot{Q}_{stn}^{HP} , \dot{Q}_{stn}^{IP} , and \dot{Q}_{stn}^{LP} to the net thermal efficiency. Figure 9a shows that the net thermal efficiency increases monotonically with the equivalence ratio for both types of biomass pretreatments. For dried biomass, the net thermal efficiency increases also with the gasification temperature, but an opposite trend is shown for torrefied biomass. Figure 9b shows that the HP steam represents the largest contribution to the net steam-power production for the overall plant. As shown in Figure 9c, the net IP steam production is negative, which indicates that the steam required by gasification is higher than the net steam produced from WGS. The LP steam production is proportional to the total conversion rate in the FT synthesis and, as shown in Figure 9d, exhibits the same dependence on the gasification

process conditions and on the type of biomass pretreatment as the biocrude production efficiency.

Electric Efficiency. Figure 10 shows the variation of the net electric efficiency, including and excluding CO_2 compression after capture, within the operational range of the EF gasification and for both biomass pretreatment systems. The net electric efficiency is here calculated from $\epsilon_{el} = (\dot{P}_{el}^{ST} + \dot{P}_{el}^{GT} - \dot{P}_{el}^{cons})/\dot{H}_F$, where \dot{P}_{el}^{ST} and \dot{P}_{el}^{GT} are the electric power production from the steam turbines and the gas turbine and \dot{P}_{el}^{cons} is the total electric power consumption by the plant. Figure 10 shows a general increase in net electric efficiency as λ_g and T_g increase, mainly due to higher HP steam production from the syngas cooling system. However, when using torrefied biomass with low λ_g values, below 0.25, the net electric efficiency increases with decreasing values of T_g . This indicates that, for torrefied biomass, the electricity production using the off-gas from the FT synthesis is dominant relative to the contribution from the HP steam generated in the syngas cooling system. When excluding the CO_2 compression train, the use of torrefied biomass leads to higher electric efficiencies than dried biomass. This is mainly due to the reduction in the power consumption associated with particle size reduction. When including the electricity consumed by the CO_2 compression train, drying of biomass leads to high electric-power efficiencies in the entire range of λ values. This can be explained since torrefied biomass has a high carbon to hydrogen ratio which results in higher CO_2 concentrations for the CO_2 capture train.

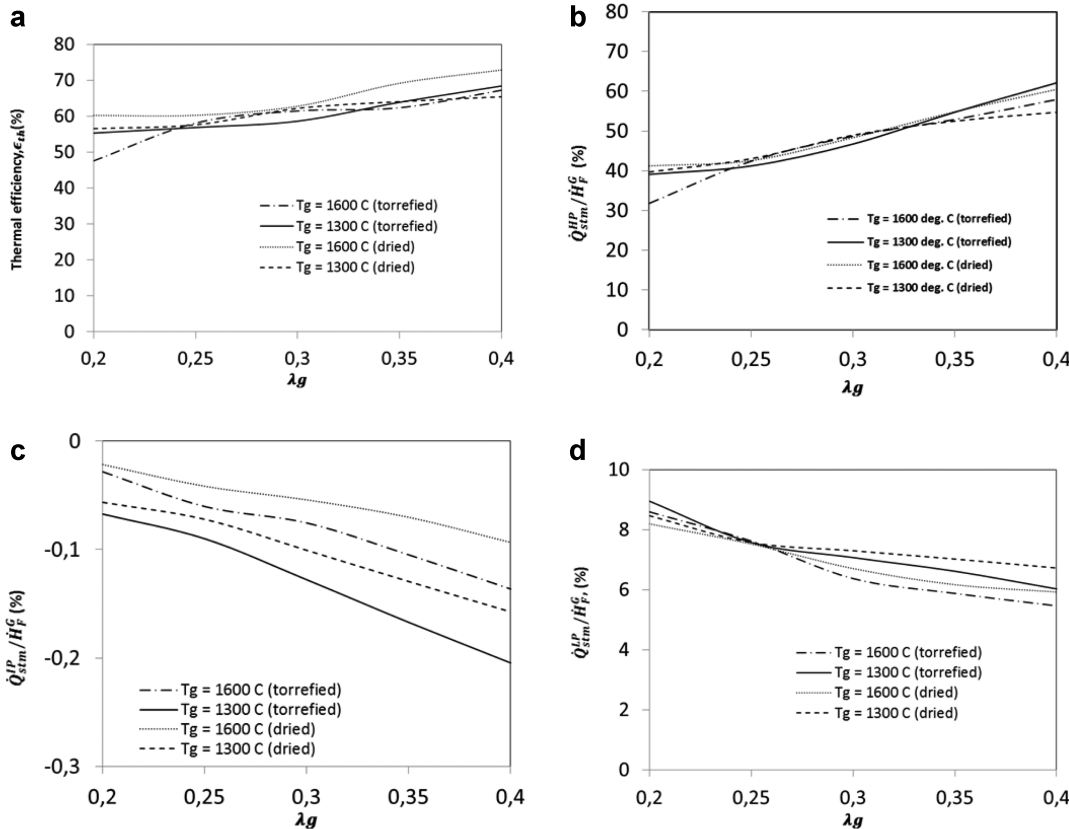


Figure 9. (a) Variation of the net steam-power production efficiency and (b) the contribution from high-pressure (HP) steam, (c) intermediate pressure (IP) steam, and (d) low-pressure (LP) steam with the gasification equivalence ratio (λ_g), both for dried and torrefied input biomass and for the range of gasification temperature considered.

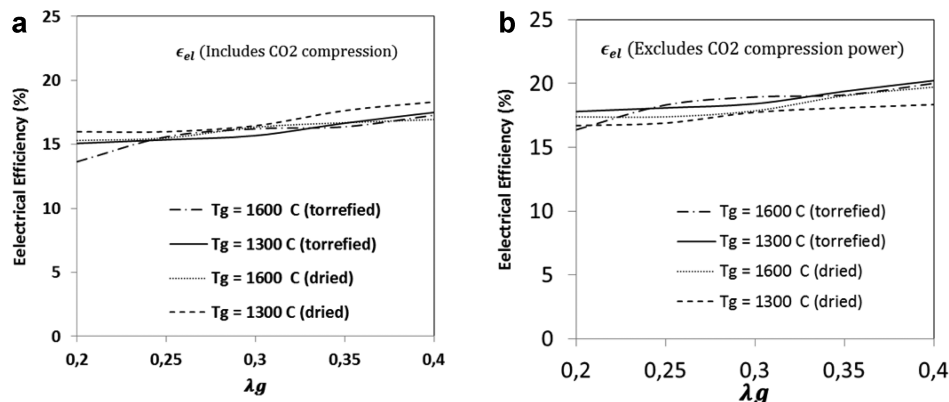


Figure 10. Variation of the net electric-power production efficiency including (a) and excluding (b) electric power consumption by the CO₂ compression train.

3. ECONOMIC ANALYSIS

In this section, the economic performance of the biocrude production plant is performed in terms of the total investment cost, the total annual operating cost, and the economic viability. The economic analysis evaluates both the influence of the main operating conditions as well the plant configuration in terms of the type of biomass pretreatment, the inclusion or exclusion of the CO₂ compression train, and the heat to electricity production ratio.

3.1. Total Permanent Investment. The total permanent investment for the biocrude production plant is evaluated from

$$C_{TPI} = \left(\sum_i C_{S,I,i} \right) [1 + f_{site} + f_{building} + f_{land}] \\ [1 + f_{cont} + f_{eng}] [1 + f_{dev} + f_{com}] \quad (6)$$

where $(\sum_i C_{S,I,i})$ is the purchase and installation cost for the overall plant calculated as the sum of purchase and installation cost of the individual equipment; f_{site} represents the cost factor associated with civil work for site preparation and access; $f_{building}$ represents the cost factor associated with buildings construction and services; f_{land} is the cost factor due to land use; f_{eng} is the cost factor due to project engineering; f_{cont} is the contingency margin; f_{dev} is the cost factor due to project development,

royalties, and patents; and f_{com} is the cost factor due to plant commissioning. Representative values for all the cost factors included in eq 7 are listed in Table 3.^{39,40}

Table 3. Cost Associated Factors to Estimate the Total Permanent Investment [eqs 8, 9]

cost associated factors	abbreviation	value
site preparation	f_{site}	0.05–0.2
buildings	f_{building}	0.05–0.1
land	f_{land}	0.05–0.1
cost of contingency	f_{cont}	0.05–0.15
engineering	f_{eng}	0.02–0.05
project development and licenses	f_{dev}	0.02–0.03
commissioning	f_{com}	0.1

Evaluation of the purchase and installation cost for each piece of equipment, C_{S_i,I_i} , has been performed using a modification of the Guthrie–Ulrich method⁴⁰ to include cost variation with pressure, materials, and required auxiliary systems, i.e., electric system, piping and valves, instrumentation and control, through simple multiplication factors. For each piece of equipment i , the purchase and installation cost is then evaluated from

$$C_{S_i,I_i} = f_{P,i} f_{\text{mat},i} f_{\text{inst},i} C_{S_b,I_b,i} (S_i/S_{b,i})^{m_i} (I/I_{b,i}) k_t^{n_i - n_{b,i}} \quad (7)$$

where C_{S_i,I_i} is the equipment purchase and installation cost evaluated for the actual equipment size S_i and cost index I_i , $C_{S_b,I_b,i}$ is the equipment purchase cost for a base-case equipment size $S_{b,i}$ and base cost index $I_{b,i}$, m_i is the equipment scale index, $f_{P,i}$ is the pressure factor, $f_{\text{mat},i}$ is the material factor, f_{inst} is the installation factor, and $k_t^{n_i - n_{b,i}}$ is the train cost factor⁴¹ for the n_i train number relative to the reference base train number $n_{b,i}$ with the parameter k_t assumed to be constant equal to 0.9.⁴² The train cost factor takes into account that for trains of multiple equipment units, the purchase and installation cost per unit decreases as the number of units in the train reduces. This is because multiple-unit trains typically share machinery and personnel during fabrication and installation and share auxiliary equipment. The cost index used in this study is based on the Chemical Engineering Plant Cost Index (CEPCI). The pressure factor $f_{P,i}$ accounts for variations in fabrication costs with the equipment design pressure P_i , which affects the material thickness and the man-hours for welding and weld testing. In this work, an exponential variation of the pressure factor, $f_{P,i} = (P_i/P_{b,i})^{k_p}$ with k_p equal to 2.208 is used based on data from Chen et al.⁴³ The installation factor has been evaluated from $f_{\text{inst},i} = 1 + f_{M,i}[1 + (L/M)_i k_L]$, with $f_{M,i}$ and $(L/M)_i$ representing the installation module factor and labor to module cost ratio for the equipment, respectively, and k_L is the labor factor for Norway. The module factor $f_{M,i}$ accounts for the auxiliary equipment and piping associated with specific main process equipment. Appendix 1 shows the purchase cost functions $C_{S_b,I_b,i}(S_i/S_{b,i})^m$ and the installation factors $f_{\text{inst},i}$ for all the individual equipment included in the plant design in this work. The purchase cost functions are obtained from Aspen ICARUS for standard process equipment and from the literature^{37–47} for more updated cost functions for specific equipment. Tailored cost functions have been developed for the entrained flow gasification reactor cost, by adapting the methodology from Reed et al.,⁴⁵ and for the low temperature FT reactor based on Larson et al.⁴² The individual equipment

installation factors in Appendix 1 are based on the work of Woods⁴⁴ with an updated L/M factor equal to 1.47 representing Norwegian conditions.⁴⁶

3.2. Operating Cost. The net cost of biocrude on an annual basis, C_{PROD} , is calculated from

$$C_{\text{PROD}} = C_B + C_{\text{op,d}} + C_{\text{op,i}} + C_{\text{maint}} \quad (8)$$

where C_B is the cost of the biomass supply, $C_{\text{op,d}}$ represents the total direct variable operational dependent on the total mass of biomass to biocrude conversion per annum, $C_{\text{op,i}}$ are the fixed indirect operational costs not directly dependent on the amount of biomass processed but required for having the plant running, and C_{maint} are the maintenance costs.

Cost of Biomass Supply. The cost of biomass supply can be estimated from

$$C_B = (\dot{M}_F t_{\text{prod}} / \rho_B) [c_{\text{expl}} + c_{\text{chip}} + c_{\text{tr,f}} + c_{\text{tr,L}} L_f] \quad (9)$$

where \dot{M}_F indicates the plant capacity based on the mass flow rate of biomass input (tons/h), t_{prod} is the annual production time (hours), ρ_B is the input biomass density (tons/m³), c_{expl} and c_{chip} are the forest exploitation cost and the cost for biomass chipping and storage, respectively, per unit biomass volume (m³), $c_{\text{tr,f}}$ and $c_{\text{tr,L}}$ are the fixed and distance-dependent unit transport costs per unit volume (m³) of biomass, and $L_f = 2(\dot{M}_F t_{\text{prod}} / m_{f,S})^{1/2}$ is the average biomass transport distance (km), which depends on the annual biomass conversion of the plant, with $m_{f,S}$ denoting the biomass availability per unit area (km²). Table 4 shows the values for ρ_B , t_{prod} , $m_{f,S}$, c_{expl} , c_{chip} , $c_{\text{tr,f}}$,

Table 4. Cost Associated Factors to Estimate the Total Permanent Investment^{47–49}

biomass supply variables	value
biomass density, ρ_B	400 kg/m ³
annual biomass production, $m_{B,S}$	10 tons/ha
cost round timer deliver at road, c_{expl}	200–250 NOK/m ³
cost of chipping and storage, c_{chip}	48.4 NOK/m ³
transportation cost (fixed), $c_{\text{tr,f}}$	24 NOK/m ³
transportation cost (variable), $c_{\text{tr,L}}$	0.6 NOK/m ³ /km

and $c_{\text{tr,L}}$ under Norwegian conditions^{47–49} used in this work. The variation of the cost of biomass supply per unit input biomass energy (GJ) is shown in Figure 11. The only biomass supply cost term which depends on the plant capacity is the variable transportation costs dependent on the distance for

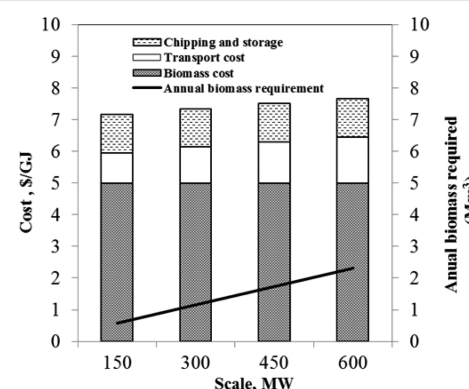


Figure 11. Supply cost of biomass sourcing from forests under Norwegian conditions.

sourcing biomass to the plant. Based on our model, for variable plant capacities in the range of 150 to 600 MW, the estimated biomass transport distance varies between 19.8 and 38 km, the transportation cost varies between 0.95 and 1.45 \$/GJ, and the overall cost of biomass supply varies from 7.2 to 7.7 \$/GJ.⁴⁸ These cost estimations are similar to those of Trømborg et al.,⁴⁸ but it depends on the type of biomass and the quality in terms of heating value, moisture content, and density.

Direct Operational Costs. Evaluation of the direct operational cost, including procurement of consumables and disposal of effluents and solid residues, was performed based on individual rates of consumption or production obtained from the mass and energy balances, the unit cost values of each specific item, and the plant annual operating time. The total direct operational costs for the plant are evaluated from

$$C_{\text{op,d}} = C_{\text{cat}}^{\text{WGS}} + C_{\text{cat}}^{\text{FT}} + C_{\text{chem}}^{\text{GC}} + \dot{M}_{\text{slag}} c_{\text{slag}} + \dot{M}_{\text{pw}} c_{\text{pw}} + \dot{M}_{\text{fw}} c_{\text{fw}} \quad (10)$$

where $C_{\text{cat}}^{\text{WGS}}$, $C_{\text{cat}}^{\text{FT}}$, $C_{\text{chem}}^{\text{GC}}$, C_{slag} , C_{pw} and C_{fw} denote the total annual costs of catalyst for WGS and FT, chemicals for gas cleaning (selexol); \dot{M}_{slag} and c_{slag} are the annual ash production and the specific cost of slag disposal per unit mass; \dot{V}_{pw} and c_{pw} are the annual volumetric (m^3) production of process water and the specific cost of process water disposal per unit volume, and \dot{M}_{fw} and c_{fw} are the annual volumetric (m^3) consumption of fresh water and the specific cost of fresh water per unit volume. Here, electricity, steam, and N_2 consumption are generated internally from the CHP and ASU systems. Other utilities such as compressed air and fuel for the auxiliary burners in the gasification reactor have been neglected. The costs of catalyst consumption are estimated from $\dot{C}_{\text{cat}}^J = n_{\text{cat}}^J (\dot{V}_g^J c_{\text{cat}}^J) / (1/\tau_{\text{cat}}^J)$ with J denoting the WGS and FT reactors, \dot{V}_g^J and $1/\tau_{\text{cat}}^J$ representing the volumetric gas flow rate and the characteristic space velocity in the catalyst bed, respectively, and c_{cat}^J and n_{cat}^J denoting the specific cost of catalyst per unit volume and the number of catalyst replacements per year. The volume of catalyst is calculated by assuming a constant gas hourly space velocity (GHSV) of 100 per hour for both the WGS and FT catalysts respectively²⁰ and that the catalyst bed is replaced after the first operating year and then every three years from the second catalyst bed. The physical solvent (selexol) is the only consumable for gas cleaning that has been included in the economic analysis, the associated cost being estimated from $C_{\text{chem}}^{\text{GC}} = n_{\text{sel}} \dot{M}_{\text{sel}}^{\text{GC}} c_{\text{sel}} \tau_{\text{sel}}$ where $\dot{M}_{\text{sel}}^{\text{GC}}$ is the mass flow rate of selexol, calculated based on a constant selexol to syngas mole ratio equal to 2.2, τ_{sel} is the total residence time of selexol in the gas cleaning system, n_{sel} is the number of selexol replacements per year, and c_{sel} is the cost per unit mass of selexol. Table 5 summarizes the reference unit values for the direct operational costs used in this work.

Table 5. Unit Values for Direct Operational Costs

direct operational cost	unit cost
slag disposal, c_{slag}	40 \$/ton ⁵⁴
WGS catalyst, $c_{\text{cat}}^{\text{WGS}}$	3.63 \$/kg ²⁰
physical solvent (Selexol), c_{sel}	5 \$/kg ⁵⁵
FT catalyst, $c_{\text{cat}}^{\text{FT}}$	13636 \$/m ³²⁰
process water disposal, c_{pw}	8.34 \$/m ³⁵⁴
fresh water, c_{fw}	0.4865 \$/m ³⁵⁴

Indirect Operational Costs. The indirect operational costs are calculated from

$$C_{\text{op,i}} = C_{\text{labor}} + C_{\text{adm}} + C_{\text{insur}} + C_{\text{tax}} \quad (11)$$

where C_{labor} is the total cost associated with all the personnel working at the plant cost, C_{adm} is the cost due to administration of the plant activity, and C_{insur} and C_{tax} are the cost for insurance and taxes, respectively. The total annual labor cost C_{labor} under Norwegian conditions can be estimated from

$$C_{\text{labor}} = c_r \sum_j N_j [f_{r,j} (1 + f_{lb}) + f_{OH,j} c_{OH}] \quad (12)$$

where c_r denotes the average hourly rate in Norway, the subscript j denotes the personnel categories, and N_j , $f_{r,j}$, f_{lb} , $f_{OH,j}$ and c_{OH} represent the annual man-hours of personnel required, the hourly rate factor, the labor burden factor, the overhead factor, and the overhead cost factor, respectively. In this work, the personnel categories included in the analysis are regular operator, skilled operator, and lab technician. The number of personnel required has been estimated based on individual process areas, i.e. fuel preparation, gasification, gas conditioning, gas cleaning, FT synthesis, CHP system, air separation unit, and other wastewater treatment areas. It is assumed that each area requires an equal number of personnel per category, two regular operators, one skilled operator, one foreman, and two lab technicians. Table 6 provides the values

Table 6. Indirect Operational Cost and Reference Values⁵⁶

indirect (fixed) operational cost	reference value
average labor hourly rate, c_r	67.9 \$/hour
operating labor burden, f_{lb}	0.3
overhead factor, $f_{OH,j}$ (operators only)	20%
labor overhead charge rate, c_{OH}	1.25
maintenance, C_{maint}	2% C_{TPI}
administration, C_{adm}	2% C_{TPI}
insurance, C_{insur}	1% C_{TPI}
income tax rate	28%

for parameters of the labor cost used in eq 12 according to Norwegian conditions. Overhead has been only considered for regular and skilled operators associated with unplanned plant shutdowns due to equipment failures. Costs for administration and insurance are evaluated as a percentage of C_{TPI} according to Table 6. The taxes for net plant income are evaluated based on a standard tax rate of 28% in accordance with industrial tax law in Norway with an additional 2% inflation.⁵⁰

Maintenance Costs. This work considers the cost of maintenance as a separate item in the overall cost of biocrude, which is evaluated from

$$C_{\text{maint}} = T_{\text{prod}} [c_{\text{spares}} + c_{\text{shut}} f_{\text{shut}}] \quad (13)$$

The first term in eq 13 represents the overall annual cost of procurement, storage, and replacement of spare parts for planned equipment wear and tear, with T_{prod} and c_{spares} denoting the plant annual production time and overall cost per unit time of spare parts. This work assumes that $T_{\text{prod}} c_{\text{spares}} \sim f_{\text{spares}} \sum_i C_{S,I,i}$ where f_{spares} is constant equal to 2%. The second term in eq 13 represents the cost of unplanned shutdowns due to unforeseen failure of equipment with c_{shut} and f_{shut} denoting the unit cost of shut down and the fraction for annual unplanned shutdown time relative to the total annual

production time for the plant. Here, c_{shut} is evaluated as the net annual income divided by the planned annual hours of operation of the plant, and f_{shut} is assumed to be 2%.

3.3. Economic Viability. Given that biomass derived biocrude will be competing mainly with the fossil based biocrude, it is necessary to assess where the system is attractive when providing biocrude at competitive prices. Analysis of the economic viability of the biocrude production plant has been performed for the case scenarios as shown in Table 9. The economic viability of the biocrude plant is assessed in the form of leveled cost⁵¹ of biocrude (denoted by C_{biocrude}), project internal rate of return (IRR). IRR can be again distinguished into project IRR which is estimated based on 100% borrowing from the bank and a financial internal rate of return or return on equity (ROE) considering investment from the investors; here we assumed 30% of the investment is coming from the project investor.

The cost of biocrude is here evaluated over the entire lifetime of the plant from

$$C_{\text{biocrude}} = \sum_{n=1}^N \left\{ \beta^n (C_{\text{TPI},n} + C_{\text{PROD},n} - C_{\text{INC},n}) \right\} / \sum_{n=1}^N \left\{ \beta^n H_{\text{bc},n} p_{\text{bc},n} \right\} \quad (14)$$

In eq 14, n is the year starting from the plant construction, N is the lifetime of the plant in years, $\beta = 1/(1+r)$ represents the time value of money with r representing the reference interest rate, $C_{\text{TPI},n}$ is the annual permanent investment $C_{\text{PROD},n}$ is the total annual production cost, $C_{\text{INC},n}$ is the total annual production cost and the total annual income from selling CHP coproducts (heat and electricity) and CO₂ credits, and $H_{\text{bc},n}$ and p_{bc} are the total annual production of biocrude on an energy basis and the annual biocrude market price.

Project IRR: Internal rate of return (IRR) is the discount rate that would make the net present value (NPV) of the investment's income stream total to zero. It is an indicator of the efficiency or quality of an investment, as opposed to net present value (NPV), which indicates value or magnitude. The present analysis is based on IRR. IRR estimated for 100% debt is called project IRR. Similarly, IRR estimated for equity ownership of 30% is called return on equity (ROE). The method is adopted from Peters et al.^{39,52} for internal rate of return analysis. The financial assumptions for evaluating C_{biocrude} and IRR are shown in Tables 7 and 8. All the plant costs are updated to the 2014 CEPCI index.⁵³ The future

Table 7. Financial Assumptions

financial parameter	values/assumptions
debt equity ratio	70–30
depreciation model	straight line depreciation model, depreciation period 20 years
construction and commissioning duration	3 year period
% required capital during construction and commissioning	30% year 1, 50% year 2, and 20% year 3
income tax rate	30%
loan repayment period	10 years
interest rate	7%
currency and reference year	\$U.S. (2014)
plant cost update	CEPCI 2014

Table 8. Operational Incomes and Reference Values

variable operational income	unit value
biocrude price	16 to 41 \$/GJ ^a
heat price	78 \$/ MWh ^c
electricity price	0.155 \$/kWh ^{c,b}
CO ₂ emissions avoided price	50–70 \$/tonne ^d
CO ₂ intensity (Norway crude oil)	6.2 gCO ₂ /MJ ⁵⁷
CO ₂ coproduct credit	50–70 \$/tonne ^e

^aVariable for sensitivity analysis. ^bSold to households, as the price of electricity for households are more compared to industry. ^cssb.no. ^dCO₂ tax varies from 240 to 300 nok/tonne according to Norwegian law, http://www.ssb.no/a/english/publikasjoner/pdf/doc_200916_en/doc_200916_en.pdf. ^ehttp://bellona.org/ccs/uploads/media/Energy_infrastructure_with_CO2_capture_and_storage_CCS_.pdf.

Table 9. Process Case Design Options

cases	case description	heat to power ratio (H-P)
case 1	influence of torrefaction as a pretreatment option and captured CO ₂ is vented to atmosphere (excludes CO ₂ compression train)	H-P:0
case 2	torrefaction scenario and includes CO ₂ capture and compression	H-P:0
case 3	drying scenario and captured CO ₂ is vented to atmosphere (excludes CO ₂ compression train)	H-P:0
case 4	torrefaction as a pretreatment and captured CO ₂ is vented to atmosphere (excludes CO ₂ compression train)	H:P:0.5
case 5	torrefaction as a pretreatment captured CO ₂ is vented to atmosphere (excludes CO ₂ compression train)	H:P:1

market price for biocrude is assumed to vary in the range 16–41 \$/GJ. The ROE as a function of crude oil price is also evaluated for the selected case by assuming 70–30 debt to equity ratio.

3.4. Results from the Economic Analysis. Techno-economics analysis of CHP integrated biocrude plant performed by establishing mass and energy balance using aspen plus for the base case of 150 MW (thermal input of biomass) as explained the previous section. Base case design consists of fuel preparation by torrefaction, followed by gasification, syngas cooling, water gas shift for gas conditioning, CO₂ separation, FT synthesis, and CHP. Alternative process case designs as shown in Table 10 are proposed to know the specific capital cost, operating cost, and cost of biocrude on the type of pretreatment options (torrefaction or conventional drying), CO₂ capture and compression train, and variations in the heat to power ratio (H-P). When the heat to power ratio is 0 (H-P:0), net steam from the high pressure, intermediate, and low pressure streams are utilized for power generation in the steam turbine cascades. When the heat to power ratio is 0.5 (H-P:0.5), 50% of the steam is utilized for the power and the other 50% is sold to the district heat network. When the heat to power ratio is 1 (H-P:1), 100% of the steam produced from the HP, IP, and LP are sold to the district heat network; in this way, a steam turbine cascade can be avoided. In this scenario, power is produced only by a gas-turbine, and a portion of the power utilized for auxiliary consumption and excess is sold. This case is very relevant to Norwegian conditions due to the availability of cheaper electricity. On the basis of this, five case designs are proposed with options of economics of scale from 150 to 600 MW of thermal input of biomass. In the Case 1, influence of torrefaction as a pretreatment option for fuel

Table 10. Product Output Biocrude, Electricity, and Heat per Year

plant capacity, MW	case 1	case 2	case 3	case 4	case 5
biocrude production in millions of liters per year (M L/ year)					
150	60	60	60	60	60
300	120	120	120	120	120
450	179	179	179	179	179
600	239	239	239	239	239
electricity production per year (MWh/year)					
150	140729	34624	110573	132539	82278
300	281459	69248	221146	265078	164557
450	422188	103872	331719	397616	246835
600	562918	138496	442292	531155	329113
heat production per year (MWh/year)					
150	0	0	0	201042	402084
300	0	0	0	402084	804168
450	0	0	0	603126	1206252
600	0	0	0	804168	1608336

preparation, and captured CO₂ is vented to atmosphere. In the Case 2, fuel preparation by torrefaction and includes CO₂ capture and compression. Case 4 follows the torrefaction scenario with variation in the heat power ratio of 0.5 (H:P:0.5), and case 5 follows the torrefaction scenario with variation in the heat power ratio of 1 (H:P:1).

3.4.1. Specific Capital Cost. Plant specific capital cost is defined by the total permanent investment C_{TPI} (\$) evaluated from eq 6, divided by the thermal capacity of the plant (kW) based on the rate of input biomass energy.

Figure 12 shows the influence of the biomass pretreatment options torrefaction versus drying, torrefaction with CO₂

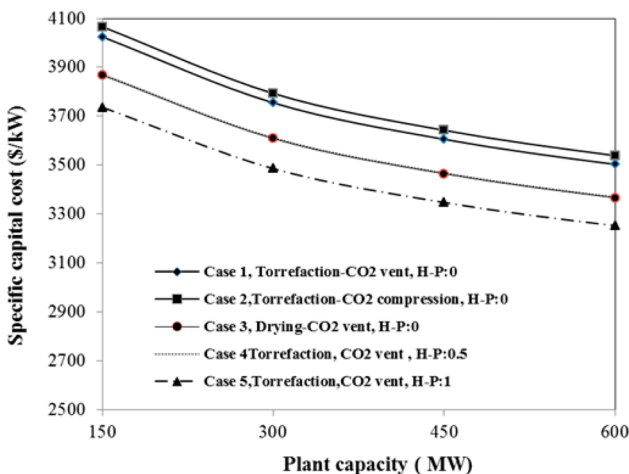


Figure 12. Influence of pretreatment options, CO₂ capture, and heat to power ratio on plant specific cost.

compression, and heat to power ratios on the specific capital cost (\$/kW) for plant capacities in the range of 150 to 600 MW. These results show an increase of approximately 3% by considering torrefaction as compared to conventional drying. The increase of specific capital cost by including compression of the CO₂ capture is very small, below 1%. There is a significant reduction in plant capital costs, about 7%, by exporting all the net steam produced from the plant for the

district heating network and, therefore, removing the steam turbine cascade system.

3.4.2. Specific Operating Cost. The plant specific operating cost is defined by the total annual operating cost C_{TPI} (\$), evaluated from eq 8 divided by the annual input biomass energy (GJ). Table 11 shows the distribution of the total annual operating costs (\$/GJ) and corresponding percentage per unit of energy of biocrude for all the cases consisting of pretreatment options as well variable heat to power ratio. The major contributors for the annual operating costs are biomass feedstock, depreciation, and labor cost, which for the scenarios with heat to power ratio of 0 contribute approximately 34, 22, and 16% of the total annual operating costs. Table 11 also shows that the increase of the heat to power production ratio from 0 to 1 leads to an increase of the coproduct credits from approximately from 7.23 \$/GJ to 19.23 \$/GJ for the same torrefaction pretreatment case scenarios, which in turn reduces significantly the net annualized operating costs. Therefore, production of heat is economically more favorable as compared to coproduction of heat and electricity.

3.4.3. Cost of Biocrude. Influence of the Process Conditions. Figure 13 shows the influence of the operating limits for the EF gasification and the CO conversion factor in the FT synthesis on the cost of biocrude for case 2 (which includes fuel preparation by torrefaction and includes CO₂ capture and compression). In general, higher λ values and temperatures in the EF gasification lead to a higher cost of biocrude mainly due to reductions on biocrude production efficiency. Increasing the CO conversion in the FT synthesis has also a significant impact on the cost of biocrude, which reduces by 50% when doubling the CO conversion in FT. Based on these results, the viability analysis presented below assumes optimal process conditions corresponding to a λ value of the EF gasification and CO conversion in FT synthesis equal to 0.25 and 80%, respectively.

Influence of the Biomass Pretreatment, Heat to Power Ratio, and CO₂ Compression. Figure 14 compares the cost of biocrude on the biomass pretreatment options, heat to power ratio, and CO₂ compression on the plant capacities in the range of 150–600 MW thermal input. Table 10 depicts the actual quantities of produced biocrude, electricity, and heat in a year for a plant capacity of 150 to 600 MW for all the cases. This result shows that using torrefaction for biomass pretreatment prior gasification can reduce the cost of biocrude by 9 to 13% compared to using conventional drying. We also depicted variations in heat to power ratio from 0, 0.5, and 1 as shown in Figure 14. The cost of biocrude decreases significantly as the heat production from the plant increases relative to electricity production. It is very relevant under Norwegian conditions since district heating is an important market and the price of electricity is low due to cheaper hydropower. We also studied one case on the influence of CO₂ compression which includes the compression train for the captured CO₂ as shown in Figure 14. Compressed CO₂ has here been considered as a coproduct that could potentially increase the income for the plant and reduce the cost of biocrude. However, including the CO₂ compression train increases the cost of biocrude by approximately 5%.

Return on Equity As a Function of Crude Oil Price for a Selected Case. Figure 15 shows the return on equity as a function of crude oil price for the selected plant capacity of 600 MW. Return on equity is estimated based on a debt-equity ratio of 70:30. These results can give an indication for investors to

Table 11. Annual Operating Costs Breakdown for Base Case 150 MW (Biomass Thermal Input)

operating components	case 1		case 2		case 3		case 4		case 5	
	H-P:0	%	H-P:0	%	H-P: 0	%	H-P: 0.5	%	H-P: 1	%
biomass feed stock	11.13	26.22	12.58	32.22	13.47	34.51	11.13	32.9	11.13	38.2
catalysts	0.56	1.31	0.66	1.69	0.63	1.61	0.56	1.6	0.56	1.9
chemicals	2.96	6.98	3.52	9.02	3.35	8.58	2.96	8.8	2.96	10.2
wastes	0.01	0.02	0.01	0.02	0.01	0.02	0.01	0.02	0.01	0.02
labor cost	6.43	15.13	6.43	16.47	6.43	16.47	6.43	19.0	6.43	22.1
maintenance	7.88	18.56	3.91	10.03	3.91	10.03	7.88	23.3	7.88	27.1
utilities	0.59	1.39	0.70	1.78	0.66	1.70	0.59	1.7	0.59	2.0
depreciation	9.20	21.65	9.29	23.79	8.84	22.63	9.20	27.2	9.20	31.6
income tax	5.67	13.35	0.00	0.01	5.41	13.85	1.63	4.8	3.16	10.9
coproduct credits	9.48	22.31	9.48	24.27	7.45	19.07	15.77	46.6	19.23	66.1
average return on investment	7.52	17.70	11.41	29.24	3.78	9.68	9.23	27.3	6.42	22.1

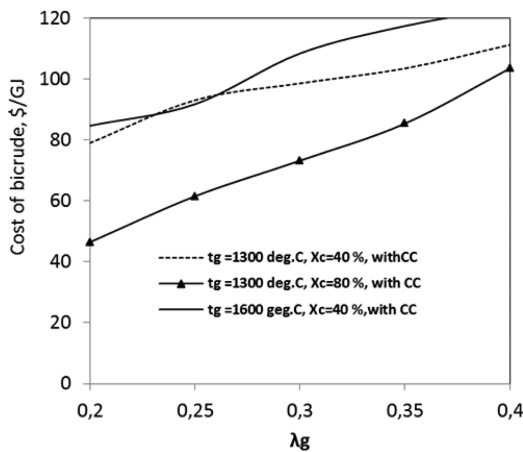


Figure 13. Effect of process operating conditions on the cost of biocrude (case 2; H-P:0).

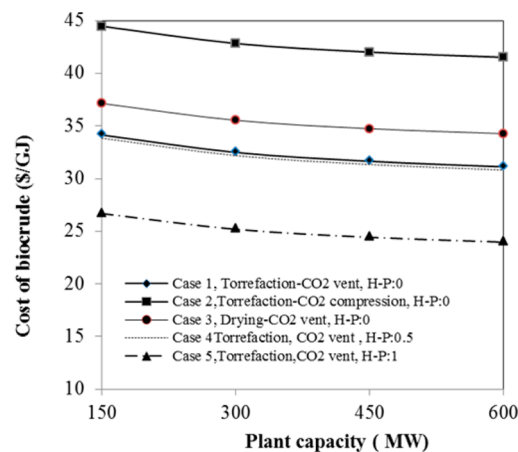


Figure 14. Variation of the cost of biocrude as a function of the plant capacity.

evaluate the economic viability of a specific project. The crude oil price has been in the range of 100 to 250 \$/barrel (17–41 \$/GJ). There is a significant increase in the return on equity as the heat to electric power production ratio increases. The plant can reap benefits with a crude selling price above 34, 37, and 41 \$/GJ for an H-P ratio of 1, 0.5, and 0, respectively.

Sensitivity Analysis. Figure 16a,b shows the results from the sensitivity analysis performed on C_{biocrude} and project IRR from

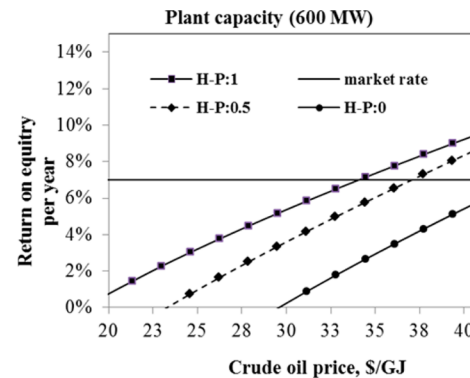


Figure 15. Return on equity as a function of crude oil price for variable heat to electricity production ratios (0, 0.5, 1) from the investor's point view.

the base cost of 24 \$/GJ. Selected parameters are electricity tariff, heat tariff, plant availability factor, total operating costs, biomass price, interest rate, slag disposal cost, percentage change in investment (TCI), biocrude production efficiency, and steam power efficiency. It can be seen that the biomass price and the total capital investment are the parameters impacting mostly the cost of biocrude and project IRR.

4. CONCLUSIONS

The influence of the process conditions and the plant process design on the economic viability of biocrude production based on EF gasification and FT synthesis with integration of CHP production has been analyzed based on detailed techno-economic analysis. The optimal process conditions are found to be λ values around 0.25 and temperatures around 1300 °C in the EF gasification. Although the use of torrefaction instead of conventional drying for biomass pretreatment increases the plant specific capital cost, this option leads to improvement in the economic viability of the plant mainly due to the higher biocrude production efficiencies achieved. Inclusion of a compression train for the captured CO₂ leads to higher specific capital costs as well as costs of biocrude. The heat to electric power production ratio has a strong influence on the economic viability of the plant. The results from this techno-economic analysis suggest that, under Norwegian conditions, export as district heating of all the residual heat produced from the main conversion process represents the optimal economic condition for the plant. Sensitivity analysis suggests that changes in

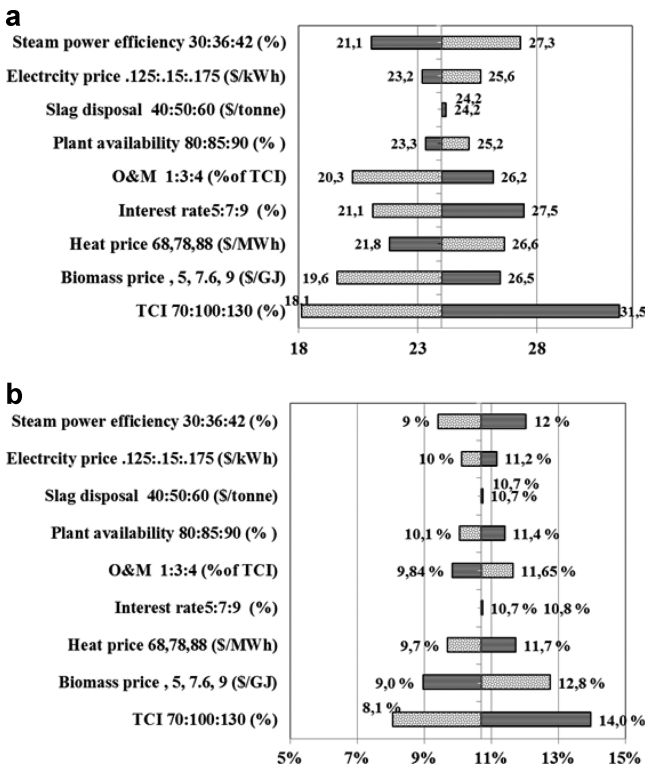


Figure 16. Sensitivity analysis on the cost of biocrude and project IRR for 600 MW capacity.

biomass price, total capital investment, interest rate, and operation and maintenance factors can influence largely the biocrude production cost.

ASSOCIATED CONTENT

Supporting Information

Appendix 1: Detailed equipment list with scaling and installation factors. This material is available free of charge via the Internet at <http://pubs.acs.org>.

AUTHOR INFORMATION

Corresponding Author

*E-mail: rajesh.kempegowda@sintef.no.

Notes

The authors declare no competing financial interest.

ACKNOWLEDGMENTS

The financial support from the Research Council of Norway and five industry partners through the project GASBIO (Gasification for biofuels) are gratefully acknowledged.

REFERENCES

- (1) Lange, J.-P. Lignocellulose Conversion: An Introduction to Chemistry, Process and Economics. In *Catalysis for Renewables*; Wiley-VCH Verlag GmbH & Co. KGaA: 2007; pp 21–51.
- (2) EU-Directive, Directive 2009/28/EC of the European Parliament and of the Council on the promotion of the use of energy from renewable sources. *Off. J. Eur. Union* 2009, 47. <http://eur-lex.europa.eu/LexUriServ/LexUriServ.do?uri=OJ:L:2009:140:0016:0062:en:PDF>.
- (3) Transport energy consumption and emissions - Statistics Explained. EUROSTAT: Luxembourg. http://epp.eurostat.ec.europa.eu/statistics_explained/index.php/Transport_energy_consumption_and_emissions.
- (4) Technology Roadmap “Biofuels for Transport.” IEA: Paris, 2009. http://www.iea.org/publications/freepublications/publication/biofuels_roadmap.pdf.
- (5) The Norwegian scenario and action plan presented by NITO Future Climate - Engineering solutions. NITO: Oslo, 2009; p 41. <http://www.fc-es.net/wp-content/themes/fces/uploads/2012/08/National-Climate-Plan-Norway-Phase-1.pdf>.
- (6) Klimaforliket – a recent Norwegian Parliament agreement on climate issues, Meld.St.21 Norsk klimapolitikk.
- (7) Strategy for increased development of bioenergy. MP&EN: 2008. <http://www.regjeringen.no/en/dep/oed/documents-and-publications/reports-2/2008/strategi-for-okt-utbygging-av-bioenergi.html?id=505401>.
- (8) Nigam, P. S.; Singh, A. Production of liquid biofuels from renewable resources. *Prog. Energy Combust. Sci.* 2011, 37 (1), 52–68.
- (9) Eisentraut, A. *Sustainable production of second-generation biofuels: potential and perspectives in major economies and developing countries*; OECD Publishing: 2010.
- (10) Singh, A.; Nigam, P. S.; Murphy, J. D. Renewable fuels from algae: An answer to debatable land based fuels. *Bioresour. Technol.* 2011, 102 (1), 10–16.
- (11) Sims, R. E. H.; Mabee, W.; Saddler, J. N.; Taylor, M. An overview of second generation biofuel technologies. *Bioresour. Technol.* 2010, 101 (6), 1570–1580.
- (12) Sadaka, S.; Negi, S. Improvements of biomass physical and thermochemical characteristics via torrefaction process. *Environ. Prog. Sustainable Energy* 2009, 28 (3), 427–434.
- (13) Felfli, F. F.; Luengo, C. A.; Suárez, J. A.; Beatón, P. A. Wood briquette torrefaction. *Energy Sustainable Dev.* 2005, 9 (3), 19–22.
- (14) Prins, M. J.; Ptasiński, K. J.; Janssen, F. J. J. G. Torrefaction of wood: Part 1. Weight loss kinetics. *J. Anal. Appl. Pyrolysis* 2006, 77 (1), 28–34.
- (15) Couhert, C.; Salvador, S.; Commandré, J. M. Impact of torrefaction on syngas production from wood. *Fuel* 2009, 88 (11), 2286–2290.
- (16) Bridgeman, T. G.; Jones, J. M.; Shield, I.; Williams, P. T. Torrefaction of reed canary grass, wheat straw and willow to enhance solid fuel qualities and combustion properties. *Fuel* 2008, 87 (6), 844–856.
- (17) Deng, J.; Wang, G.-j.; Kuang, J.-h.; Zhang, Y.-l.; Luo, Y.-h. Pretreatment of agricultural residues for co-gasification via torrefaction. *J. Anal. Appl. Pyrolysis* 2009, 86 (2), 331–337.
- (18) Phanphanich, M.; Mani, S. Impact of torrefaction on the grindability and fuel characteristics of forest biomass. *Bioresour. Technol.* 2011, 102 (2), 1246–1253.
- (19) Arias, B.; Pevida, C.; Fermoso, J.; Plaza, M. G.; Rubiera, F.; Pis, J. J. Influence of torrefaction on the grindability and reactivity of woody biomass. *Fuel Process. Technol.* 2008, 89 (2), 169–175.
- (20) Swanson, R. M.; Platon, A.; Satrio, J. A.; Brown, R. C. Techno-economic analysis of biomass-to-liquids production based on gasification. *Fuel* 2010, 89 (Supplement1, (0)), S11–S19.
- (21) Ekbom, T.; Hjerpe, C.; Hagstrom, M.; Hermann, F. *Pilot study of Bio-jet A-1 fuel production for Stockholm-Arlanda Airport*; Värmeforsk: Stockholm, 2009.
- (22) Tijmensen, M. J. A.; Faaij, A. P. C.; Hamelinck, C. N.; van Hardeveld, M. R. M. Exploration of the possibilities for production of Fischer-Tropsch liquids and power via biomass gasification. *Biomass Bioenergy* 2002, 23 (2), 129–152.
- (23) Tapasvi, D.; Khalil, R.; Skreiberg, Ø.; Tran, K.-Q.; Grønli, M. Torrefaction of Norwegian Birch and Spruce: An Experimental Study Using Macro-TGA. *Energy Fuels* 2012, 26 (8), 5232–5240.
- (24) Hernández, J. J.; Aranda-Almansa, G.; Bula, A. Gasification of biomass wastes in an entrained flow gasifier: Effect of the particle size and the residence time. *Fuel Process. Technol.* 2010, 91 (6), 681–692.
- (25) Newsome, D. S. The Water-Gas Shift Reaction. *Catal. Rev.* 1980, 21 (2), 275–318.
- (26) Olanders, B.; Steenari, B.-M. Characterization of ashes from wood and straw. *Biomass Bioenergy* 1995, 8 (2), 105–115.

- (27) Qin, K. Entrained Flow Gasification of Biomass. Ph.D, Technical University of Denmark, Denmark, 2012.
- (28) Smith, B.; Loganathan, M.; Shantha, M. S. A Review of the Water Gas Shift Reaction Kinetics. *Int. J. Chem. Reactor Eng.* **2010**, *8*, 10.2202/1542-6580.2238.
- (29) Arnold, K.; Stewart, M. *Surface Production Operations, Vol. 2:: Design of Gas-Handling Systems and Facilities*; Gulf Professional Publishing: 1999; Vol. 2.
- (30) Bridgwater, A. *Progress in Thermochemical Biomass Conversion*; John Wiley & Sons: 2008.
- (31) Daey Ouwens, C.; den Uil, H.; Boerrigter, H. Tri-generation from biomass and residues: Options for the co-production of Fischer–Tropsch liquids, electricity and heat. *Progress in Thermochemical Biomass Conversion*; Wiley: New York, 2001; pp 488–498.
- (32) Rytter, E.; Ochoa-Fernández, E.; Fahmi, A. Biomass-to-Liquids by the Fischer–Tropsch Process. *Catal. Process Dev. Renewable Mater.* **2013**, 265–308.
- (33) Dry, M. E. The Fischer–Tropsch process: 1950–2000. *Catal. Today* **2002**, *71* (3–4), 227–241.
- (34) Wender, I. Reactions of synthesis gas. *Fuel Process. Technol.* **1996**, *48* (3), 189–297.
- (35) Schulz, H. Short history and present trends of Fischer–Tropsch synthesis. *Appl. Catal., A* **1999**, *186* (1–2), 3–12.
- (36) Vhatvarothai, N.; Ness, J.; Yu, Q. J. An investigation of thermal behaviour of biomass and coal during pyrolysis using thermogravimetric analysis. *Int. J. Energy Res.* **2013**, 1145–1154.
- (37) Higman, C.; Van der Burgt, M. *Gasification*; Gulf Professional Publishing: 2011.
- (38) Anderson, R.; Friedel, R.; Storch, H. Fischer–Tropsch Reaction Mechanism Involving Stepwise Growth of Carbon Chain. *J. Chem. Phys.* **2004**, *19* (3), 313–319.
- (39) Peters, M. S.; Timmerhaus, K. D.; West, R. E.; Timmerhaus, K.; West, R. *Plant Design and Economics for Chemical Engineers*, 5th ed.; McGraw-Hill: New York, 2003; Vol. 4.
- (40) Ulrich, G. D.; Vasudevan, P. T. *Chemical Engineering: Process Design and Economics; a Practical Guide*; Process Publ.: 2004.
- (41) Martelli, E.; Kreutz, T.; Carbo, M.; Consonni, S.; Jansen, D. Shell coal IGCCS with carbon capture: Conventional gas quench vs. innovative configurations. *Appl. Energy* **2011**, *88* (11), 3978–3989.
- (42) Larson, E. D.; Jin, H.; Celik, F. E. Large-scale gasification-based coproduction of fuels and electricity from switchgrass. *Biofuels, Bioprod. Biorefin.* **2009**, *3* (2), 174–194.
- (43) Chen, C. *A Technical and Economic Assessment of Co2 Capture Technology for IGCC Power Plants*; Carnegie Mellon University: 2005.
- (44) Woods, D. R. *Rules of Thumb in Engineering Practice*; John Wiley & Sons: 2007.
- (45) Reed, M.; Bibber, V.; Shuster, E.; Haslbeck, J.; Rutkowski, M.; Olsen, M. *Baseline Technical and Economic Assessment of a Commercial Scale Fischer–Tropsch Liquids Facility*. NETL: USA, 2014.
- (46) Ereev, S.; Patel, M. *Recommended methodology and tool for cost estimates at micro level for new technologies*; Prosuite: Utrecht, Netherlands, 2011.
- (47) Trømborg, E.; Bolkesjø, T. F.; Bergseng, E.; Rørstad, P. *Bærekraftig Biodrivstoff Til Sivil Luftfart I Norge - Biomassetilgang Fra Landbaserte Ressurser*; Institutt for naturforvaltning, Universitetet for Miljø- og Biovitenskap: 2012.
- (48) Trømborg, E.; Havskjold, M.; Lislebø, O.; Rørstad, P. K. Projecting demand and supply of forest biomass for heating in Norway. *Energy Policy* **2011**, *39* (11), 7049–7058.
- (49) Analyse og Strategi: Bærekraftig biodrivstoff til sivil luftfart i Norge - delutredning 3: Lokalisering av prosessanlegg for produksjon av biodrivstoff, inklusive logistikkanalyse In 2012; Avinor: Oslo, 2012.
- (50) KPMG Corporate tax rate. <http://www.kpmg.com/global/en/services/tax/tax-tools-and-resources/pages/corporate-tax-rates-table.aspx> (March 2014).
- (51) Short, W.; Packey, D. J.; Holt, T. *a Manual for the Economic Evaluation of Energy Efficiency and Renewable Energy Technologies*; University Press of the Pacific: 2005.
- (52) Towler, G. P.; Sinnott, R. K. *Chemical Engineering Design: Principles, Practice, And Economics of Plant and Process Design*; Elsevier: 2013.
- (53) CEPCI Chemical Engineering. Economic Indicators, 2014. www.che.com.
- (54) Enabling advanced pre-combustion capture techniques and plants: European best practice guidelines for assessment of CO₂ capture technologies in 2011; DECARBit: Trondheim, Norway, 2011; p 99.
- (55) Chen, C.; Rubin, E. S. CO₂ control technology effects on IGCC plant performance and cost. *Energy Policy* **2009**, *37* (3), 915–924.
- (56) Eurostat Labour costs in the EU28. http://epp.eurostat.ec.europa.eu/cache/ITY_PUBLIC/3-27032014-AP/EN/3-27032014-AP-EN.PDF.
- (57) *Carbon Intensity of Crude Oil in Europe*; ICCT: Washington, DC, 2013 http://www.climateworks.org/imo/media/doc/ICCT_crudeoil_Eur_Dec2010_sum.pdf.